





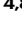


# Discrete Immolative Guanidinium Transporters deliver mRNA to specific organs and red blood cells

Received: 19 December 2024

Accepted: 16 July 2025

Published online: 01 August 2025



Zhijian Li <sup>1,11</sup>, Aloysius Ee<sup>1,2,3,11</sup>, Laura Amaya <sup>4,5,11</sup>, Jennifer L. Hamad <sup>1,6</sup>, Pavan K. Yadav<sup>1</sup>, Sean K. Wang <sup>4,7</sup>, Howard Y. Chang <sup>4,8,10</sup> & Paul A. Wender <sup>1,9</sup> 

RNA medicine is an emerging groundbreaking technology for the prevention and treatment of disease. However, tools to deliver messenger RNA (mRNA) and other polyanions (circRNA, saRNA, pDNA, CRISPR-Cas, reprogramming factors) are required to advance current RNA therapies and address next generation challenges. Existing delivery systems often suffer from laborious syntheses, limited organ selectivity, formulation complexity, and undesired inflammatory responses. Here, we report novel mRNA delivery systems termed Discrete Immolative Guanidinium Transporters (DIGITs), which are synthesized convergently in as few as 4 steps. Unlike most cationic (ammonium) delivery systems, DIGITs are based on cationic guanidinium moieties, which complex mRNA at acidic pH and undergo irreversible neutralization at physiological pH to enable efficient RNA release. Systematic evaluation of structural variations and formulations have led to DIGIT/mRNA complexes that selectively target lung, spleen, and immature red blood cells in peripheral blood in female mice model. DIGIT/mRNA delivery systems show minimal toxicity based on cell viability and biochemical assays, supporting their future utility in biomedical applications.

The global impact of COVID-19 mRNA vaccines on human health and the subsequent recognition of this research by the Nobel Prize Committee have ushered in a rapidly advancing age of RNA therapeutics<sup>1</sup>. Emerging post-Covid applications are being directed at a vast array of medical problems including infectious disease<sup>2,3</sup>, cancer immunotherapy<sup>4</sup>, prophylactic and therapeutic vaccinations<sup>5–7</sup>, genome editing<sup>8</sup>, protein replacement therapies<sup>9</sup>, and regenerative medicine<sup>10</sup>. The successful implementation of the next generation of mRNA therapeutics will require more effective systems to deliver RNA

to desired organs and cell types with high efficiency and minimal toxicity. Toward these goals, lipid nanoparticles (LNP) represent especially attractive delivery systems, and much progress has been made in recent years to enhance LNP-mediated mRNA delivery to the liver<sup>9</sup>, lungs<sup>11,12</sup>, spleen<sup>11,12</sup>, and other organs<sup>13,14</sup>. However, some top performing LNP formulations have been reported to elicit inflammatory responses, which could complicate clinical use beyond vaccine applications<sup>5–7</sup>. Moreover, the requirement of multiple delivery components (typically 4–5) poses additional challenges for formulation

<sup>1</sup>Department of Chemistry, Stanford University, Stanford, CA, USA. <sup>2</sup>Department of Materials Science & Engineering, Stanford University, Stanford, CA, USA.

<sup>3</sup>College of Engineering, Nanyang Technological University, 70 Nanyang Drive, Singapore, Singapore. <sup>4</sup>Center for Personal Dynamic Regulomes, Stanford University, Stanford, CA, USA. <sup>5</sup>Institute for Stem Cell Biology and Regenerative Medicine, Stanford University School of Medicine, Stanford, CA, USA.

<sup>6</sup>Department of Biology, Stanford University, Stanford, CA, USA. <sup>7</sup>Department of Ophthalmology, Stanford University School of Medicine, Stanford, CA, USA.

<sup>8</sup>Howard Hughes Medical Institute, Stanford University, Stanford, CA, USA. <sup>9</sup>Department of Chemical and Systems Biology, Stanford University, Stanford, CA, USA. <sup>10</sup>Present address: Amgen Research, South San Francisco, CA, USA. <sup>11</sup>These authors contributed equally: Zhijian Li, Aloysius Ee, Laura Amaya.

 e-mail: [wenderp@stanford.edu](mailto:wenderp@stanford.edu)

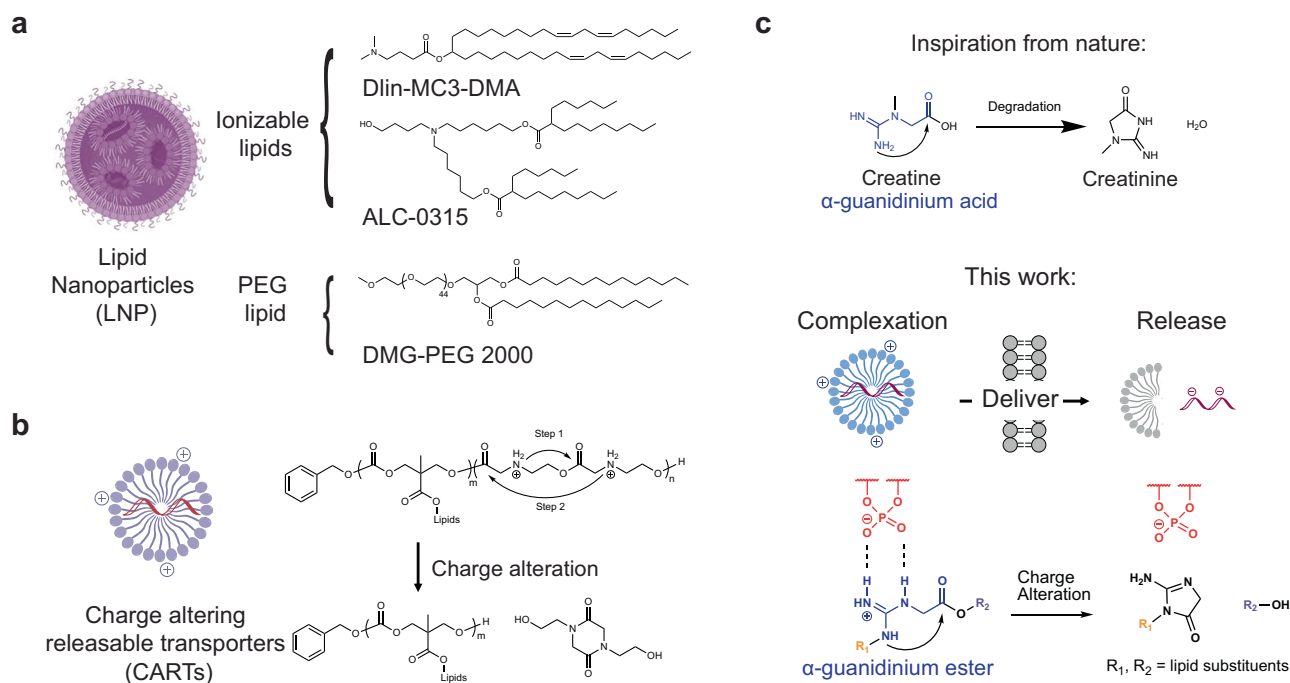


**Fig. 1 | Various non-viral strategies to deliver mRNA efficiently in vivo.**

**a** Representative structures of ionizable lipids (generally protonated amines) and PEG lipids used in FDA approved LNP formulations. Created in BioRender. Zhang, R. (2025) <https://BioRender.com/c7fq80>. **b** Representative structure of CARTs and

development and the manufacturing process of RNA drug products, especially in scenarios in which delivery of multiple RNA cargos is necessary to achieve optimal therapeutic effect<sup>7,15</sup>. To address this limitation, recent LNP studies have reported formulations containing fewer components<sup>16,17</sup>.

The Chang, Levy, Waymouth, and Wender groups have reported the design, development, and in vitro and in vivo evaluation of self-immolative LNPs for RNA/DNA delivery called Charge-Altering Releasable Transporters (CARTs)<sup>18</sup> (Fig. 1b). CARTs are formed in two steps involving an organocatalytic oligomerization of a lipid monomer initiated by an alcohol followed by oligomerization of a second monomer which, upon deprotection, provides a second (charged) block. The resulting oligomeric CARTs form stable electrostatic complexes with mRNA at acidic pH (<5.5), but at physiological pH (~7.4) rapidly undergo an O- to N-acyl shift, irreversibly producing neutral small molecules and releasing the RNA/DNA cargo. Variations in the initiator and lipid and charged components of CARTs have resulted in efficient delivery of mRNA<sup>19</sup>, siRNA<sup>20</sup>, and circRNA<sup>21</sup> in vivo to various organs and cell types, leading to pre-clinical advancement toward multiple biomedical applications (e.g., COVID-19 vaccine, prophylactic and therapeutic vaccinations against cancer in mice, CAR-T and CAR-NK cell engineering and therapies)<sup>15,22,23</sup>. Most recently, CARTs furnished with self-immolative guanidinium groups have been reported for tunable organ selective delivery and for the development of cancer vaccines in mice<sup>24</sup>. Notably, CARTs elicit minimal inflammatory responses and toxicity in pre-clinical models<sup>15,22</sup>. This is likely due to the unique degradation process that neutralizes positive charges known to trigger coagulation cascade and inflammatory cytokine release<sup>25</sup>.

While oligomeric CART delivery systems have proven to be effective, the use of discrete charge-altering transporters has not been explored. As single entities, discrete transporters are hypothesized to be easier to characterize with reduced batch-to-batch variations,

the charge altering mechanism enabling RNA release. **c** Creatine bearing an  $\alpha$ -guanidinium motif undergoes cyclization in vertebrate metabolism, a mechanism which could be repurposed to complex, deliver, and release mRNA cargos. Drawings in (a–c) were created with ChemDraw.

facilitating their production, evaluation, clinical translation, and regulatory approval. Moreover, unlike the vast majority of ammonium based LNP formulations, discrete transporters would exploit the avidity of guanidinium groups to complex RNA cargos without any other additives, greatly simplifying formulation development and manufacturing processes. However, a key to the implementation of this idea is whether discrete transporters/RNA complexes could be designed to undergo pH responsive charge cancellation, which would liberate their polyanionic cargos.

Our approach to address the charge cancellation problem was inspired by  $\alpha$ -guanidinium acids, such as creatine, a substantial metabolite in the human body (~120 g for a 70 kg adult)<sup>26</sup> (Fig. 1c) which along with its phosphorylated derivative are responsible for ATP generation in skeletal muscles. Interestingly, creatine is known to irreversibly cyclize into creatinine and needs to be replenished by diet or de novo synthesis<sup>26,27</sup> (Fig. 1c). The tendency of creatine to cyclize with a loss of charge prompted us to investigate whether  $\alpha$ -guanidinium esters (AGE) could be employed as a novel cationic motif for RNA delivery and release (Fig. 1c). Building on our seminal work on guanidinium-rich cell penetrating transporters<sup>28,29</sup>, we and others have shown that guanidinium groups form relatively strong bidentate hydrogen bonds and electrostatically associate with negatively charged oxyanions (e.g. mRNA, siRNA, phospholipids, carboxylates, sulphates), suggesting AGE could complex with mRNAs and facilitate their cellular uptake<sup>28,29</sup>. While the avidity of this association would interfere with cargo release, cyclization of AGE would provide a mechanism for charge cancellation and RNA release, a process observed in some prodrug release studies<sup>30,31</sup>. Further enthusiasm to investigate this RNA delivery concept arose from the expected facile and convergent synthesis of  $\alpha$ -guanidinium esters ( $R_1$ ,  $R_2$ ), which would enable the attachment of diverse lipid substituents which have proven to be important for nanoparticle formation, cellular uptake, endosomal escape, and organ and cell tropism<sup>32</sup>.

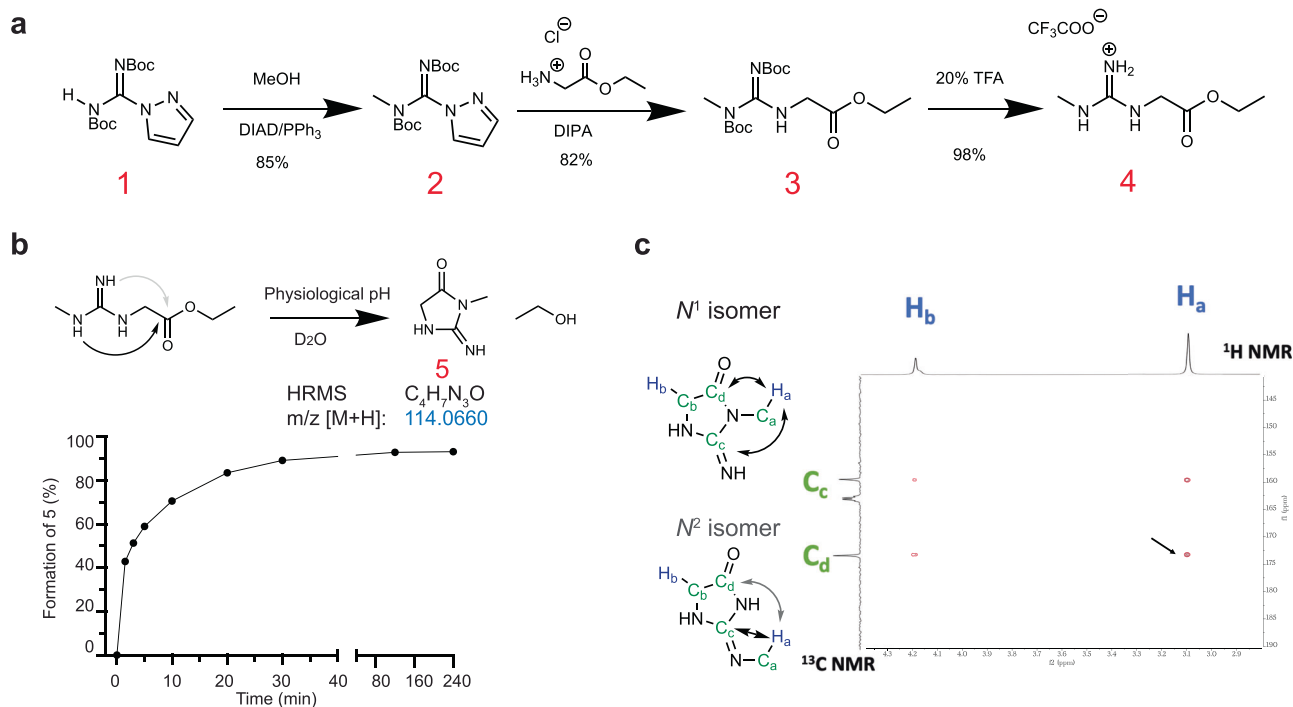


**Fig. 2 | Synthesis and charge neutralization of  $\alpha$ -guanidinium esters (AGE).** **a** Synthesis of model substrate **4** to investigate AGE degradation. **b** Formation of **5** monitored by  $^1\text{H}$  NMR. **c** Regioselectivity of cyclization characterized by  $^1\text{H}$ - $^{13}\text{C}$

HMBC.  $\text{H}_a$ - $\text{C}_d$  coupling was detected (black arrow), which can only occur when the  $\text{N}^1$  isomer is formed.

Here we report a novel class of mRNA delivery systems, discrete (non-oligomeric) immolative guanidinium transporters (DIGITs), leveraging on the unique chemical properties and reactivities of AGEs. DIGITs are discrete guanidinium-containing esters, in other words pure, single agents and the first of their kind to undergo charge cancellation. As pure entities DIGITs are more scalable, easier to characterize, and easier to tune and do not suffer from batch-to-batch variations that is encountered with many oligomeric systems. These features provide significant regulatory, cost, and research advantages. Here we show that DIGITs form stable complexes with mRNA at acidic pH while undergoing a rapid ester-to-acylguanidine cyclization leading to charge neutralization of the guanidinium group and release of the mRNA cargo, at physiological pH (Fig. 1c). Synthesized as discrete entities in as few as 4 steps, a library of 38 DIGITs with varying lipid substituents were prepared and characterized. Variation of chemical structures and formulation conditions enabled us to identify DIGITs that selectively delivered mRNA to the lungs (94% selectivity), spleen (98% selectivity), and immature red blood cells in peripheral blood (86% selectivity, 12% reticulocyte transfection) upon intravenous (retro-orbital) administration with superior efficiency over previously reported CART systems. Notably, DIGITs showed minimal inflammatory response and toxicity, supporting their potential use in biomedical applications.

## Results

### Synthesis and pH-responsive charge neutralization of $\alpha$ -guanidinium esters (AGE)

We first set out to evaluate the degradation behavior of AGE at physiological pH using a model substrate **4** (Fig. 2a) in the absence of a polyanionic (RNA) cargo. Toward this end, carboxamidine **1** was efficiently methylated to yield **2** via published Mitsunobu procedures<sup>33</sup>. **2** was coupled with glycine ethyl ester using a modified procedure<sup>34</sup> to yield **3** which was subsequently deprotected to give **4** as a TFA salt. **4** was stable in unbuffered  $\text{D}_2\text{O}$  for at least 2 days (pH = 2.0) at room

temperature. The solution pH was then adjusted to a physiological range (pH = 7.4) with  $\text{Na}_2\text{CO}_3$ , and the degradation of **4** was monitored by  $^1\text{H}$  NMR (Fig. 2b). The cyclic product **5** formed rapidly (~50% conversion at 3 min) along with ethanol as the byproduct (Fig. 2b, Supplementary Fig. 1). The degradation mixture was purified by HPLC and the chemical identity of **5** was established by NMR and mass spectrometry. The regioselectivity of the cyclization was determined by  $^1\text{H}$ - $^{13}\text{C}$  HMBC NMR (Fig. 2c), which demonstrated that the  $\text{N}^1$  isomer was formed ( $\text{H}_a$ - $\text{C}_d$  coupling). This observation aligns with a previous report showing that passing **4** through a weakly basic ion exchange column yielded the  $\text{N}^1$  isomer<sup>35</sup>. These results demonstrate that the AGE motif featured in DIGITs could undergo charge neutralization in a pH-dependent manner.

### Synthesis and characterization of discrete immolative guanidinium transporters (DIGITs)

Having established the charge-altering behavior of AGE, we next set out to synthesize a library of DIGITs to evaluate their use as polyanion (RNA) delivery systems. Toward this end, Boc-protected glycine esters **6** and functionalized carboxamidines **7** were prepared from lipid alcohols ( $\text{R}_1\text{-OH}$ ,  $\text{R}_2\text{-OH}$ ) in one step in high yields, respectively (Fig. 3a). TFA deprotection of **6** and subsequent treatment of **7** with base yielded Boc protected DIGITs **8**, which upon TFA deprotection provided the DIGITs as TFA salts. This convergent synthetic strategy enabled us to access DIGITs with diverse lipid structures from commercially and synthetically accessible lipid alcohols in as few as 4 steps. Using this strategy, we constructed 2 DIGIT libraries (**10Gx** and **yG10**) in which lipid #10 (selected based on our experience<sup>19</sup>) was always present on one side of the DIGIT (Fig. 3b). 38 DIGITs in total were synthesized (**10G1-10G20**, **1G10-18G10**, **BNT**) with 21 types of lipid attachments (Lipid #1-21) encompassing various lipid classes including linear-saturated (#1-3), branched (#4-14)<sup>19</sup>, unsaturated (#15-16)<sup>36</sup>, amine-containing (#17), cyclic (#18-20)<sup>37</sup>, and lipids used in the COVID-19 vaccine LNP formulations (#21)<sup>38</sup> (Fig. 3b). For example, **10G9** refers

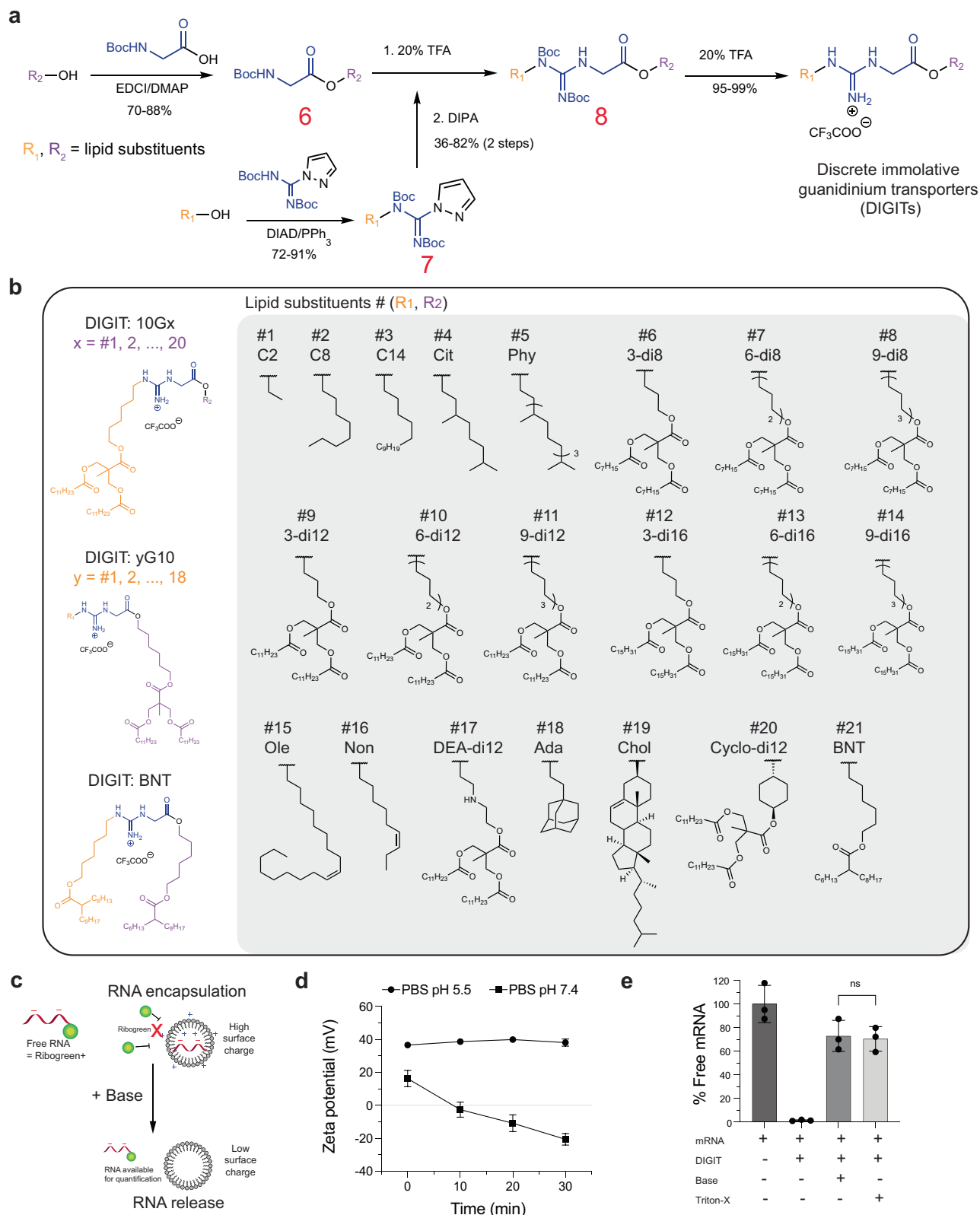


**Fig. 3 | Convergent synthesis of DIGIT libraries and characterization of DIGIT/mRNA complexes. a** Convergent synthesis of DIGITs from lipid alcohols. **b** Chemical structure of lipid substituents and the resulting DIGIT libraries evaluated in this study. yGx = DIGIT structure attached with lipid #y on the guanidinium side (orange) and with lipid #x on the ester side (purple). **c** Scheme to evaluate DIGIT/mRNA complexes and their degradation (surface charge and RNA

encapsulation). Created with ChemDraw. **d** Surface charge of DIGIT/mRNA complexes over time incubated in buffers with different pH ( $N=3$ ). Data are presented as mean values  $\pm$  SD. **e** Evaluation of mRNA encapsulation and release by Ribogreen assay ( $N=3$ ). Data are presented as mean values  $\pm$  SD. Mann Whitney test was applied,  $P$ -value  $> 0.999$ . ns = not significant. Source data are provided as a Source Data file.



to the DIGIT structure where lipid #10 is attached on the guanidinium side (orange) and lipid #9 is attached on the ester side (purple). By varying the lipids on the opposite side of the AGE core, we efficiently explored the chemical space and the impact of lipid asymmetry (e.g., **10G9** v.s. **9G10**) on delivery efficiency and selectivity<sup>39,40</sup> (Fig. 3b). We hypothesize that lipid asymmetry could modulate the delivery efficacy of DIGITs because different degradation products are generated following charge alteration. As indicated in Supplementary Fig. 2, DIGIT **10G9** and **9G10** degrade into different cyclic acyl guanidines and different alcohols. As is seen with multicomponent delivery systems, these structural variations could impact cellular uptake, endosomal escape, and RNA release of DIGIT/RNA nanoparticles. All DIGITs were synthesized in 20–200 mg scales with 29–58% overall yields from lipid alcohols ( $R_1$ -OH,  $R_2$ -OH) as the starting materials.

We then evaluated the ability of the individual DIGITs to complex, deliver, and release an mRNA cargo in vitro (Fig. 3c). DIGIT **10G9** was formulated with mRNA encoding firefly luciferase (mfluc) in acidified PBS buffer (pH 5.5) and PBS (pH 7.4) at a 5:1 charge ratio (guanidinium: RNA phosphate). The surface charge of each nanoparticle was monitored over time by a Zetasizer. While remaining positive in acidic buffer, the surface charge of the DIGIT/mRNA complexes decreased under physiological conditions (pH 7.4) (Fig. 3d), indicating the loss of cationic charge, consistent with our results in the AGE charge neutralization study. We then set out to determine if the degradation of DIGIT/mRNA complexes correlate with mRNA release using a Ribogreen assay, in which a fluorescent dye selectively binds to free mRNA but not to encapsulated mRNA. The use of **10G9** resulted in >98% mRNA encapsulation in acidified PBS buffer (Fig. 3e). In contrast, but in line with pH-based release, increasing the pH of the DIGIT/mRNA formulation with a base led to approximately 70% recovery of the fluorescence signal. (Fig. 3e). The extent of mRNA release was similar to DIGIT/mRNA complexes treated with Triton-X (0.5%), an established detergent used in LNP studies to disassemble nanoparticles<sup>41</sup>. These results support the hypothesis that DIGITs could complex and release mRNA in a pH-responsive manner.

### DIGITs selectively deliver mRNA to the lungs and/or spleen, and the tropism can be controlled by the formulation buffers

Stability in blood is crucial for intravenous administration, as extensive degradation would prevent delivery and expression. To evaluate the stability and delivery efficiency of DIGIT complexes in vivo, we first performed intravenous delivery of naked mRNA which resulted in no detectable protein expression, while DIGIT formulations induced expression levels three orders of magnitude higher than the PBS control (Supplementary Fig. 3a). This indicates that DIGIT complexes are stable enough in the bloodstream to facilitate the delivery of mRNA. As blood circulation time is short (seconds to <5 minutes in mice)<sup>42,43</sup>, the complexes have sufficient time to target distinct organs before degradation occurs. Additionally, we incubated DIGIT/mfluc nanoparticles with plasma and monitored their sizes, which did not change significantly up to 30 min (Supplementary Fig. 3b). This suggests that DIGIT formulations could potentially be stabilized by protein corona formation effects in the blood.

DIGIT/mfluc complexes were formulated by simple pipette mixing of the two components in acidified PBS buffer (pH 5.5, 20% sucrose) without the need for any additives. The resulting complexes were administered to mice via retro-orbital intravenous injection (Fig. 4a). Whole body bioluminescence signals of luciferase activity were quantified (Fig. 4b, Supplementary Fig. 4). We observed that most top performers have branched lipid tails on both sides of the guanidinium-ester core (lipid # 6-14), consistent with findings from LNP studies that indicate larger lipid volume enhances delivery efficiency<sup>44</sup>. In general, formulations at a 5:1 charge ratio resulted in higher luciferase expression except for **15G10** and **16G10** formulations. The DIGIT analog with BioNTech lipids exhibited lower performance

relative to others, which could be attributed to the lack of additional components such as helper lipids, cholesterol, and PEG-lipids needed for standard LNP formulations. We also observed notable differences in delivery efficiency between structural isomers that differed only by the site of lipid attachments (e.g. **10G9** v.s. **9G10**) (Supplementary Fig. 4). Additionally, we observed a weak positive correlation between DIGIT hydrophobicity (CLogP) and nanoparticle size with delivery efficiency for formulations with a 5:1 charge ratio (Supplementary Fig. 5). This correlation was weaker in formulations with a 12.5:1 charge ratio (Supplementary Fig. 5). To provide further analysis on structure-function relationships, we analyzed variants with fork lipid tails on both sides (**6G10-14G10**, **10G6-10G14**). These structures generally demonstrated superior delivery efficiency compared to DIGITs with other lipid attachments. As shown in Supplementary Fig. 6, lipid tails with 12 carbons performed better while linker length had no discernible effect on delivery efficiency. These findings highlight the importance of lipid tail composition in enhancing the functionality of DIGITs for mRNA delivery.

We isolated organs from mice to further characterize the organ selectivity of the top performers (Fig. 4c). At a 5:1 charge ratio, **10G9**, **10G14**, and **17G10** formulations exhibited highly selective spleen tropism (up to 98%). **10G9** resulted in luciferase protein expression of up to 5.7-fold higher than ONA CART<sup>36</sup> (our previous positive oligomeric benchmark) and minimal expression in the liver (Supplementary Fig. 7). In addition to spleen targeting, we sought to identify strategies for lung targeting given its importance in various diseases, such as respiratory diseases<sup>45</sup>. Previous studies suggested that charge ratio increase could promote mRNA delivery to lungs<sup>24,46</sup>. However, increasing the charge ratio for DIGITs (including **10G9**) from 5:1 to 12.5:1 failed to elicit lung delivery (Supplementary Fig. 8). We therefore decided to investigate the effect of buffers on DIGIT formulations, which have been observed to improve LNP efficiency for intravenous<sup>47</sup> and nebulized delivery<sup>46</sup>. Remarkably, a simple change of buffer from acidified PBS (pH 5.5) to NaOAc buffer (11 mM, pH 3.5) led to a drastic tropism shift from spleen (98%) to lung (94%) with the **10G9** formulation at the 12.5:1 charge ratio (Fig. 4d). Variation in salt composition and concentration also favored lung tropism (Supplementary Fig. 9). The composition of acidified PBS and NaOAc buffers differed in various aspects, including pH, buffer salt type, and amount of NaCl. Systematic screening revealed that NaCl content was solely responsible for the observed tropism shift. NaCl-containing buffers (e.g. PBS pH 5.5) promoted spleen tropism, whereas buffers lacking NaCl favored lung tropism (Fig. 4e). We also identified significant differences in nanoparticle size of DIGIT formulations (Fig. 4e), suggesting that the buffers could induce tropism shifts by affecting the biophysical properties of nanoparticles. This observation, which to the best of our knowledge has not been reported before, could also be observed in several other DIGITs (Supplementary Figs. 10, 11).

To further characterize the unexpected tropism shift observed with DIGITs, we determined if organ tropism of other lipid nanoparticle formulations (e.g., SM-102 4-component system) could also be affected by buffer composition. In Supplementary Fig. 12, we showed that buffers with or without sodium chloride didn't significantly change tissue tropism, even though protein expression was affected. This suggested that the mechanism of tropism shift for DIGITs and lipid nanoparticles could be different. This is not unexpected as guanidinium cations and buffer anions are bidentate coordinators while ammonium cations (e.g., SM-102) and chloride are mono-dentate coordinators. We hypothesize that buffer composition (e.g., anions) could affect the biophysical properties of resulting nanoparticles.

To determine cell populations transfected in the organs, we formulated **10G9** with 10  $\mu$ g Cre mRNA and administered the resulting nanoparticles to mice with Cre/lox-P cassettes<sup>48</sup>. Successful delivery and expression of Cre mRNA in cells induces tdTomato expression, which is visualized by fluorescence microscopy and

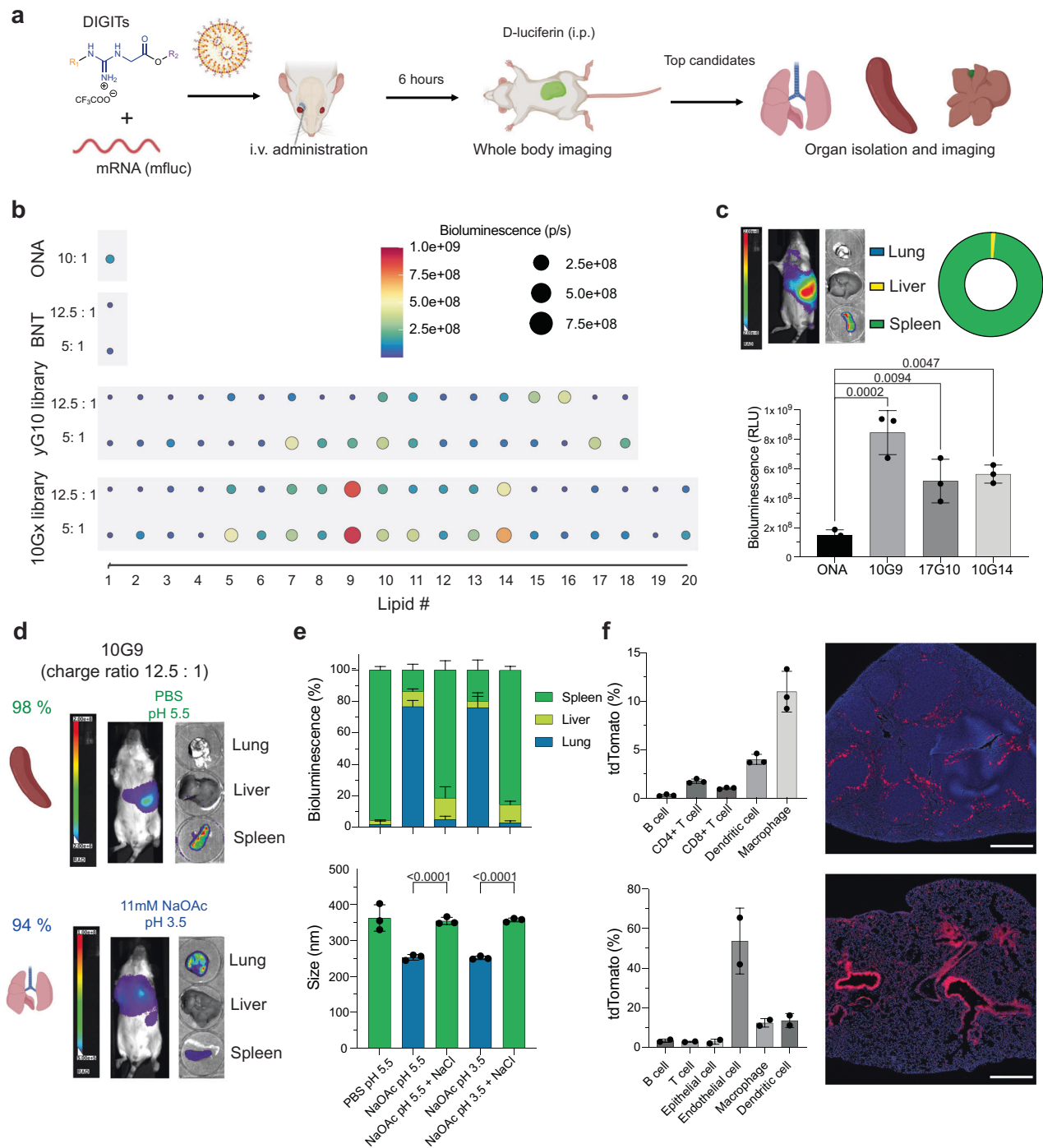


**Fig. 4 | In vivo assessment of DIGIT/mRNA complexes: organ tropism and transfection efficiency.** **a** Schematic representation of mfluc delivery in vivo to assess the biodistribution of protein expression. Created in BioRender. Zhang, R. (2025) <https://BioRender.com/c7fqb80>. 5 μg (0.25 mg/kg) mfluc was complexed with each DIGIT and delivered retro-orbitally. **b** Whole body bioluminescent signals (N=2) for DIGITs formulated with mfluc at 5:1 and 12.5:1 charge ratio. **c** Organ selectivity and delivery efficiency of spleen-tropic DIGIT/mfluc complexes (N=3). Data are presented as mean values ± SD. Ordinary one-way ANOVA was applied for multiple comparison test. **d** Shift of organ tropism of 10G9 (charge ratio 12.5:1) by changing formulation buffers of DIGIT/mRNA complexes. Created in BioRender.

Zhang, R. (2025) <https://BioRender.com/c7fqb80>. **e** Effect of buffer composition and pH on organ tropism (top, N=3), and the corresponding sizes (bottom, N=3) of nanoparticles. Data are presented as mean values ± SD. Ordinary one-way ANOVA was applied for multiple comparison test. **f** Composition of transfected cells in the spleen (top, N=3) and lung (bottom, N=2) in the Ai14 mouse model with DIGIT/Cre mRNA complexes evaluated by flow cytometry (left) and fluorescence microscopy (right). Data are presented as mean values ± SD. Scale bar = 500 μm. Source data are provided as a Source Data file. Illustrations of lung and spleen in (d, f) were created in BioRender. Zhang, R. (2025) <https://BioRender.com/c7fqb80>.

quantified by flow cytometry (Fig. 4f, Supplementary Fig. 13). Upon analysis of distinct cell types, lung endothelial cells (CD45- CD31+) and splenic macrophages (CD45+ F480+) were the most prominently transfected (Fig. 4f, Supplementary Fig. 14). The transfection

profile resembled our previous study with GSer-CARTs<sup>24</sup>, suggesting that the two delivery systems could share similar mechanisms of delivery. The proximity of endothelial cells and splenic macrophages to blood flow in the lungs and spleen, respectively, may explain the

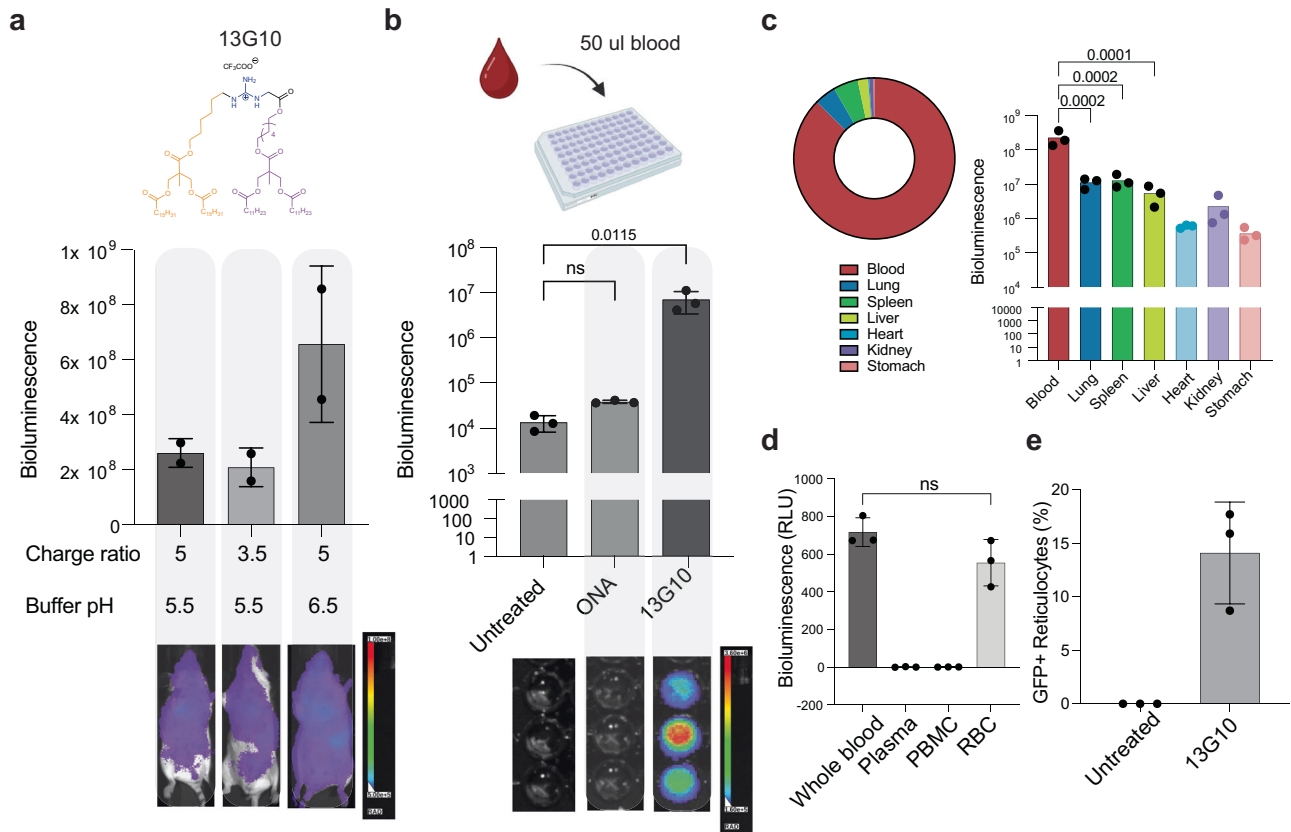


**Fig. 5 | In vivo analysis of blood-specific mRNA delivery using DIGIT complexes.** **a** Optimization of leading blood-tropic DIGIT formulation ( $N=2$ ). Data are presented as mean values  $\pm$  SD. **b** Evaluation of luciferase signal in blood ( $N=3$ ). Data are presented as mean values  $\pm$  SD. Ordinary one-way ANOVA was applied for multiple comparison test.  $P$  value = 0.999. ns = not significant. Icons (top) created in BioRender. Zhang, R. (2025) <https://BioRender.com/c7fq80>. **c** Calculated selectivity of blood transfection from isolated organs ( $N=3$ ). Data are presented as

mean values  $\pm$  SD. Ordinary one-way ANOVA was applied for multiple comparison test. Blood signal (Blood) was estimated by multiplying signal on plate reader by 32-fold (1600  $\mu$ l blood for animal/50  $\mu$ l). **d** Luciferase signal in different murine blood components after administration of **13G10**/mfluc complex in vivo ( $N=3$ ). Data are presented as mean values  $\pm$  SD. Mann Whitney test was applied.  $P$ -value = 0.2000, ns = not significant. **e** Transfection of reticulocytes after administration of **13G10**/eGFP mRNA complex in vivo ( $N=3$ ). Source data are provided as a Source Data file.

preferential delivery observed, a phenomenon that will be the focus of future studies.

We benchmarked lung-tropic and spleen-tropic DIGITs against GSer-CARTs, a polymeric system with demonstrated therapeutic potential<sup>19</sup>. We demonstrated that lung tropic DIGITs had similar delivery efficiency and selectivity (94% for DIGIT v.s. 96% for GSer-CART) compared to lung tropic GSer-CARTs (Supplementary Fig. 15a, b). On the other hand, spleen tropic DIGITs resulted in 2.1-fold greater protein expression and similar selectivity (98% for DIGIT v.s. 97% for GSer-CART) compared to spleen tropic GSer-CARTs (Supplementary Fig. 15c, d).

Representative DIGITs from each category (lung-tropic, spleen-tropic, and blood-tropic) were selected to evaluate encapsulation efficiency, surface charge in acidic buffers, and surface charge changes in physiological buffers (Supplementary Figs. 16 and 17).

To assess size uniformity and batch reproducibility, two independent batches of DIGIT **10G9** were synthesized and formulated with fluc mRNA. No significant differences were observed in nanoparticle sizes or in vivo delivery efficiency between the batches (Supplementary Fig. 18). This consistency highlights the advantage of DIGITs as discrete systems, which minimize batch-to-batch variation and enhance their potential for clinical translation.

### DIGITs selectively deliver mRNA to immature red blood cells

Published mRNA transporters predominantly induce protein expression in localized organs (e.g., lung, liver, spleen). Surprisingly, we noticed that several DIGIT/mfluc formulations lead to systemic

expression (e.g., **13G10**, Supplementary Fig. 4), which prompted further optimization of this novel delivery option for blood delivery applications. The delivery efficacy of the **13G10**/mfluc complex was further optimized by varying its charge ratios and formulation buffers (Fig. 5a). We postulated that the whole-body expression patterns could stem from transfection of cells in peripheral blood. Indeed, blood isolated from mice administered with **13G10**/mfluc complexes resulted in robust bioluminescence upon incubation with D-luciferin solution (Fig. 5b), while the blood from untreated mice and mice treated with spleen-tropic ONA CART showed no detectable signal (Fig. 5b). 86% of the luciferase signal occurred in peripheral blood, indicating that the **13G10** formulation is highly selective for blood transfection (Fig. 5c).

We next sought to determine what type of cells were transfected in the blood. Surprisingly, the bioluminescence signal was completely quenched when ACK lysis was carried out to deplete the red blood cells (Supplementary Fig. 19), a common procedure implemented prior to flow cytometry analysis. To ensure the signal loss was not due to inhibition of luciferase activity by lysis buffers, we isolated individual blood components (plasma, peripheral blood mononuclear cells, and red blood cells) via density gradient centrifugation with established Ficoll techniques and incubated them with D-luciferin solution. Remarkably, the luciferase signal was exclusively retained in the red blood cell (RBC) pellet with > 270-fold selectivity over plasma and peripheral blood mononuclear cells (PBMCs) (Fig. 5d). While mature RBCs lack ribosomes for mRNA translation, peripheral blood consist of 1-5% immature RBCs (also called reticulocytes)<sup>49</sup>. Devoid of nuclei,



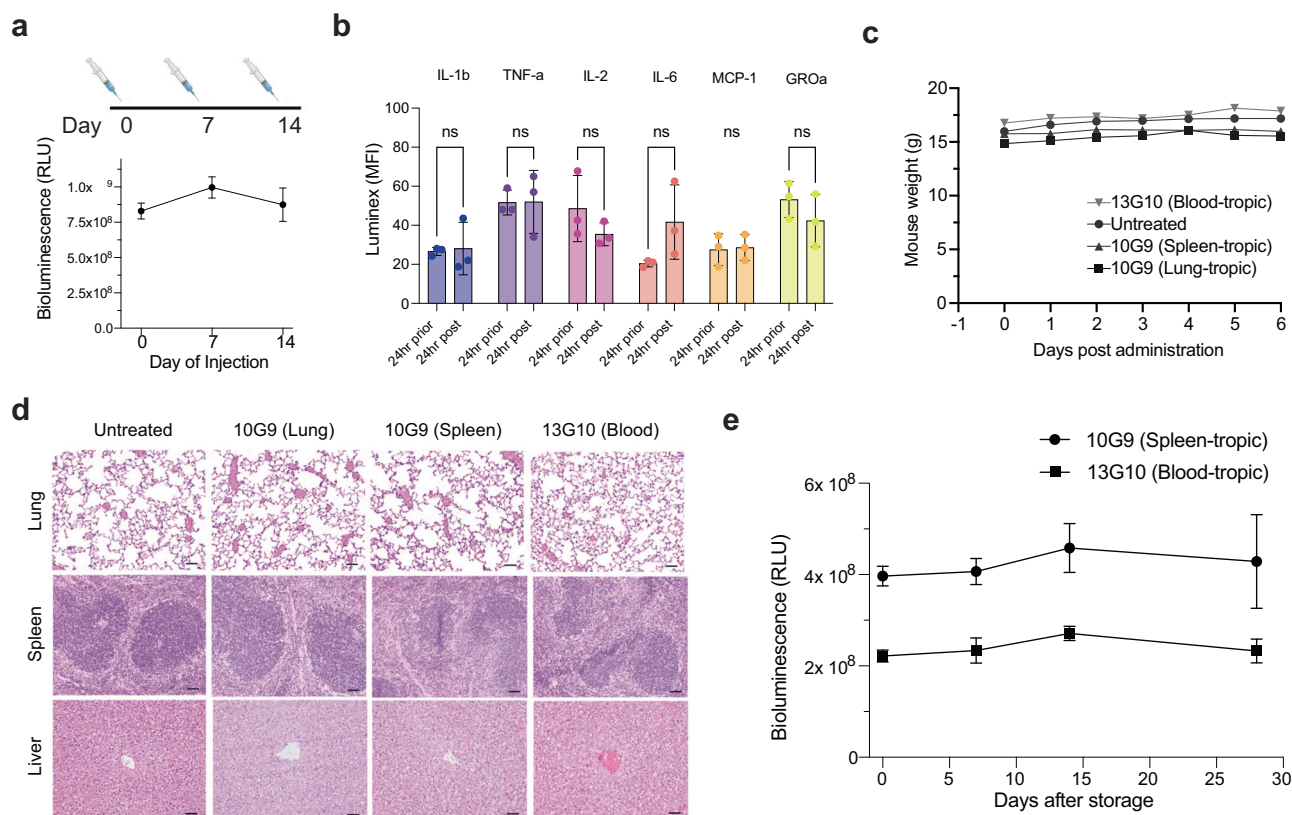


**Fig. 6 | Assessing the safety, efficacy, and stability of DIGIT/mRNA complexes.** **a** Redosing mice with DIGIT/mfluc formulations for 3 consecutive weeks (0.25 mg/kg) ( $N=3$ ). Data are presented as mean values  $\pm$  SD. Illustrations created in BioRender. Zhang, R. (2025) <https://BioRender.com/c7fq80>. **b** Levels of inflammatory cytokines before and after administration of DIGIT/mRNA complexes (0.5 mg/kg) ( $N=3$ ). Data are presented as mean values  $\pm$  SD. Two-way ANOVA was applied for multiple comparisons testing.  $P$ -values =  $>0.9999$ ,  $>0.9999$ , 0.6686,

0.1714,  $>0.9999$ , 0.8273. ns = not significant. **c** Weight change in mice after administration of DIGIT/mRNA complexes. ( $N=3$ ). Data are presented as mean values  $\pm$  SD. **d** H&E staining of isolated organs 1 week after administration of DIGIT/mRNA complexes (20x mag, scale 50  $\mu$ m). **e** Luciferase protein expression of DIGIT/mRNA complexes freshly prepared (Day 0) or stored at  $-80^{\circ}\text{C}$  for given days ( $N=3$ ). Data are presented as mean values  $\pm$  SD. Source data are provided as a Source Data file.

reticulocytes contain all the machineries needed for protein translation and could potentially be the target for mRNA delivery. We therefore administered mice with **13G10** complexed with 7.5  $\mu$ g of eGFP mRNA, to evaluate the biodistribution of protein expression. Encouragingly, 12% of reticulocytes (Ter119 + CD71 +) exhibited eGFP expression (Fig. 5e, Supplementary Fig. 20), while transfection of PBMCs and splenocytes showed minimal expression ( $<1\%$ ) (Supplementary Fig. 21). These results indicate that DIGIT formulations could transfect reticulocytes with high efficiency and selectivity and result in systemic distribution of expressed agents.

#### DIGIT delivery resulted in minimal toxicity and inflammation

In addition to efficiency and selectivity, assessing the effect of delivery on the host is also crucial for successful clinical translation. For example, while viral delivery systems are efficient vectors for gene therapies, they typically induce deleterious host immune responses and have limited use in applications requiring repeated dosing. Encouragingly, we administered DIGIT/mfluc complexes once per week over three weeks and observed consistent robust protein expression (Fig. 6a). To determine if DIGIT delivery is immunogenic, we measured inflammatory cytokine levels before and after DIGIT/mfluc administration and found no significant difference (Fig. 6b). Finally, the overall health of the treated animals was also monitored, and a complete necropsy study was performed by expert veterinarians. Mice did not exhibit weight loss upon administration of DIGIT/mfluc formulations (Fig. 6c), and no tissue damage was identified from hematoxylin and eosin (H&E) staining of isolated tissues a week after

administration (Fig. 6d). In addition, we have conducted blood count studies, and observed comparable levels of red blood cells and reticulocytes in circulation between animals administered the DIGIT/mRNA complexes and standardized metrics of healthy ranges (Supplementary Table 1). These results together support DIGITs as non-inflammatory and safe vehicles for mRNA delivery in murine models.

To address potential concerns regarding the generation of alcohol byproducts during mRNA release, we conducted a hemolytic assay on the alcohol generated from DIGIT degradation showing that it does not induce red blood cell lysis ( $<1\%$ ) (Supplementary Fig. 22). These results collectively indicate that DIGIT complexes exhibit favorable safety and hemocompatibility profiles.

To further support the use of DIGITs in clinical application and the stability of the chemical structures, we investigated the long-term stability of the DIGIT/RNA formulations. We observed that formulated DIGIT/mRNA complexes could be stored at  $-80^{\circ}\text{C}$  without losing their delivery efficiency for the duration of the study (4 weeks) (Fig. 6e).

#### Discussion

Designed cell-penetrating guanidinium-rich transporters for drug delivery were introduced in 2000<sup>28,50</sup>. While effective for gene delivery, these guanidinium-rich peptides and peptoids required lengthy syntheses<sup>51</sup>. Subsequent studies addressed this problem using a two-step organocatalytic route to produce guanidinium-rich oligomers<sup>29</sup>. These worked for siRNA delivery<sup>29</sup> but failed for longer polyanions (e.g., mRNA) due to the avidity of the guanidinium-anion association which prevented intracellular polyanion release. This problem with



cargo release led to the abandonment of guanidinium cationic complexation and the introduction of CARTs based on charge cancelling oligomers of lipidated-ammonium cations<sup>18,36</sup>. Here we return to guanidinium cation complexation and report in vivo RNA delivery with designed discrete immolative guanidinium transporters (DIGITs) which undergo irreversible pH-determined charge cancellation enabling release of their polyanionic cargo. Being discrete systems as opposed to oligomeric mixtures, DIGITs offer greater control over structure, synthesis, and properties and thus delivery optimization and clinical translation. DIGITs and their formulations, including the unusual effect of buffer, offer exquisite control of cell and organ tropism without a targeting ligand. The dynamic chemical properties of DIGITs enable stable RNA complexation upon formulation and efficient RNA release upon delivery with minimal toxicity. The facile and convergent synthesis of DIGITs with diverse lipid attachments provides a platform for addressing various delivery problems as demonstrated herein with the identification of candidates exhibiting selective lung, spleen, and blood delivery upon intravenous administration. DIGIT/RNA complexes do not elicit inflammatory responses in murine models and therefore represent effective and safe delivery candidates for a variety of clinical applications.

Our findings also highlight the unique capability of DIGITs to target reticulocytes, which is not found with GSer-CARTs. This further demonstrates the advantages of discrete systems for selective cell-type delivery and the possibilities for using this platform for biomedical applications. The development of delivery systems that target red blood cells offers exciting clinical potential for therapeutic and diagnostic applications. Due to the natural abundance, long lifespan, and unique trafficking properties of RBCs, novel strategies could be developed to exploit these features, including the use of RBCs for brain-targeted cell therapies and for novel diagnostic tools. One promising application is the delivery of small interfering RNAs (siRNA) targeting BCL11A for the treatment of hemoglobinopathies such as sickle cell disease and  $\beta$ -thalassemia. RBC-based delivery systems could also be used to deliver therapeutics across the blood-brain barrier (BBB), a major obstacle in the treatment of neurological diseases. Finally, RBCs could offer a non-invasive and cost-effective approach for disease monitoring. For example, RBCs loaded with biosensors or molecular probes could circulate in the bloodstream, detecting biomarkers associated with cancer, cardiovascular diseases, or infectious agents.

## Methods

### Chemical synthesis and degradation study of alpha amino ester motifs

Synthetic procedures for all compounds and the procedure to study AGE degradation can be found in the supplementary information.

### Ribogreen assay to evaluate mRNA encapsulation and release

Acidified PBS buffer (pH 5.5, termed “PBS 5.5” hereafter) was prepared from PBS buffer (pH 7.4) and pH adjusted with HCl solution, followed by addition of sucrose (20% w/v). Sucrose was used as a cryoprotectant and stabilizing agent. Quant-iT RiboGreen RNA Reagent (ThermoFisher, R11491) was diluted 1:100 in the PBS 5.5 buffer. To measure mRNA encapsulation efficiency, DIGITs (15–40 mM in DMSO) were added to PBS 5.5 buffer containing 420 ng of luciferase mRNA (Trilink L-7211, 5MoU) at 5:1 charge ratio. After 30–35 times of pipette mixing, the formulation (8.4  $\mu$ l) was diluted to 100  $\mu$ l with deionized (DI) water and transferred to a black 96 well plate (Fisher Scientific, 12-566-70). 10  $\mu$ l of diluted Ribogreen solution was added and mixed for 10 times and the fluorescence signal was measured with a plate reader (Spectramax id3, excitation = 480 nm, emission = 520 nm). To measure mRNA release, 8.4  $\mu$ l 100 mM aqueous  $\text{NaHCO}_3$  or 0.5% Triton-X was added and mixed with the DIGIT formulation before dilution with DI water, and the fluorescence signal was recorded as described above.

### Dynamic light scattering (DLS) for size analysis and Zeta-potential for surface charge analysis

For size and zeta potential measurements in acidic formulation buffer, DIGITs were added to PBS 5.5 with 20% sucrose containing 420 ng of luciferase mRNA (Trilink L-7202, 5MoU) at various charge ratios indicated above (cation: anion). The formulations were mixed for 20 seconds using a micropipette (drawing and dispensing 8  $\mu$ l about 3 times/second) and subsequently diluted with 1 mL of DI water. The dilutions were then immediately transferred to a disposable clear plastic cuvette, and the sizes measured by NanoBrook Omni (Serial No: 280097). Surface charge was monitored at 0, 10, 20, and 30 min after formulation using the same instrument. For zeta potential measurements in physiological pH, DIGIT/mfluc formulations were prepared as described above. 8.4  $\mu$ l 100 mM  $\text{NaHCO}_3$  (pH 8) were added and mixed for 10 s and subsequently diluted with DI water for measurement. The resulting mixture was diluted in 1 mL of DI water and its pH was measured with a pH meter ( $\sim$ 7.4). For plasma incubation experiments, DIGIT/mfluc formulations were prepared as described above. 8.4  $\mu$ l plasma (balb/c) was added to the formulation and mixed for 5 s and the resulting nanoparticle sizes monitored over 30 minutes.

The nanoparticle sizes of all DIGIT formulations were characterized and summarized in Supplementary Table 2 and Supplementary Table 3 for direct comparison.

### In vivo mRNA delivery

All mice in this study were maintained under specific pathogen-free conditions, 12 light/12 dark cycle, temperatures of  $-18$ – $23$  °C with 40–60% humidity, and handled according to the protocol (Protocol ID: 14046) approved by the Institutional Animal Care and Use Committee (IACUC) of Stanford University. Female BALB/c mice (000651) were purchased from Jackson Laboratory and housed in the Laboratory Animal Facility of the Stanford University Medical Center. The mice were matched for sex and aged between 8 and 14 weeks. Two to three animals were used per experimental condition.

### Luciferase mRNA biodistribution

DIGITs were complexed with 5  $\mu$ g of Luciferase mRNA (Trilink L-7202, 5moU) in PBS 5.5 to a total volume of 100  $\mu$ l at a 5:1 or 12.5:1 N:P ratio following the same formulation procedure described above. The formulations were mixed for 20 seconds using a micropipette (drawing and dispensing 100  $\mu$ l twice/second) before retro-orbital injections. 6 hours after injection, D-luciferin solution (100  $\mu$ l, 30 mg/mL) was injected intraperitoneally, and whole-body luminescence was measured using the AMI Imaging system CCD camera and analyzed with Aura. To evaluate luciferase expression in blood, retro-orbital bleeding was performed and 50  $\mu$ l blood was pipetted into a black 96 well plate for imaging. Mice were subsequently sacrificed in  $\text{CO}_2$  for 8 min and their lungs, livers, spleens, hearts, kidneys, and stomachs were isolated to quantify organ specific luciferase expression.

### Ail4 Cre-mediated recombination

Female Ail4 mice ( $\sim$ 20 g, week 8) were purchased from Jackson Laboratory and housed in the Laboratory Animal Facility of the Stanford University Medical Center. DIGITs were complexed with 10  $\mu$ g of Cre mRNA (Trilink L-7211) in PBS 5.5 to a total volume of 100  $\mu$ l with the same formulation procedure described above. Spleens and lungs were isolated 48 h after transfection to measure Cre-mediated recombination. Spleens were smashed with a 100  $\mu$ m strainer to make a single-cell suspension. Lungs were digested with collagenase type IV (Worthington) at a concentration of 1 mg/ml for 20 min at 37 °C, and then passed through a 100  $\mu$ m strainer to obtain a single-cell suspension. Red blood cells were lysed before staining. Single-cell samples were then stained with Zombie NIR (BUV570, BioLegend 423103), anti-CD45 (clone 145-2C11, BioLegend), anti-CD8 $\alpha$  (clone 53-6.7, BioLegend), anti-CD4 (clone RM4-5, BioLegend), anti-CD11c (clone IM7, BioLegend),

anti-CD19 (clone 30-F11, BioLegend), anti-F4/80 (clone H1.2F3, BioLegend), anti-CD31 (eF450, BioLegend), and anti-CD326 (Pe-Cy7, BioLegend). Cells were then washed twice and analyzed by flow cytometry. Data were collected on a Attune NXT Flow Cytometer.

For the imaging of transfected tissues, isolated lungs and spleens were fixed with 4% paraformaldehyde overnight at 4 °C, washed with PBS, cryoprotected in PBS with sucrose, and frozen in a 1:1 mixture of optimal cutting temperature compound (Tissue-Tek) and PBS with 30% sucrose. Cryosections were cut 20  $\mu$ m thick, stained with DAPI to label cell nuclei, and mounted onto glass slides using Vectashield antifade mounting media (Vector Laboratories). Images were acquired on a Keyence BZ-X fluorescence microscope using a 2x or 20x air objective lens.

### Evaluation of blood-tropic DIGIT/mRNA formulations

For bioluminescence studies, DIGIT **13G10** was complexed with 5  $\mu$ g of mfluc in PBS 5.5 as described above and administered intravenously. 6 h post injection, 50 (for Fig. 5b, c)–200  $\mu$ l (for Fig. 5d) of blood was collected via retro-orbital bleeding. For ACK lysis, 200  $\mu$ l blood was incubated with 3 mL of ACK lysis buffer for 10 min at room temperature. After centrifugation the cell pellet was resuspended in 200  $\mu$ l of PBS 7.4 (2% FBS) containing 300  $\mu$ g of D-luciferin and luminescence was measured on a plate reader. Alternatively, different blood cell subsets were isolated by density gradient centrifugation and analyzed separately. Briefly, 200  $\mu$ l blood was diluted with 200  $\mu$ l PBS 7.4 (2% FBS) and carefully layered on 375  $\mu$ l of Ficoll media. Isolated plasma, PBMC, and RBC pellets (resuspended in 200  $\mu$ l of PBS 7.4 with 2% FBS) were transferred to a 96 well plate and incubated with 10  $\mu$ l of 30 mg/mL D-luciferin substrate before plate reader analysis.

For flow cytometry analysis, **13G10** was complexed with 7.5  $\mu$ g of eGFP mRNA. 6 hr post-injection, 200  $\mu$ l of blood was collected and blood components were isolated as described above by gradient centrifugation. RBC pellets (diluted 1:2000), PBMC pellets (diluted 1:100), and splenocytes (diluted 1:500) were stained with stained with anti-CD45 (PerCP, BioLegend), anti-CD71 (APC, BioLegend), anti-CD11b (BV510, BioLegend), and anti-Ter119 (BV786, BioLegend). Cells were then washed twice and analyzed by flow cytometry. Data were collected on a Attune NXT Flow Cytometer.

### Preclinical toxicology analysis

Mice were dosed with 10  $\mu$ g of luciferase mRNA complexed with DIGIT. Animals were then monitored daily for general health and body weight.

Blood samples were collected 24 h after treatment. Blood samples collected 24 h after DIGIT/mRNA injection were processed to isolate serum for Luminex analysis conducted by the Human Immune Monitoring Center at Stanford University. This analysis was performed using the Mouse 48 plex Procarta kit (Thermo Fisher/Life Technologies) following manufacturer instructions.

Histopathological analysis was also conducted on these animals 24 h after treatment. Animals were sent to the Comparative Pathology Medicine Center at Stanford University to be evaluated for potential treatment-related effects by experienced veterinary pathologists. Lesions in the liver, kidney, and thymus were evaluated compared to an untreated control. Representative histological images were collected for the liver, lung, and spleen for each experimental group.

### Stability of encapsulated DIGIT/mRNA

To monitor any degradation or loss of efficacy of the mRNA complexed with DIGIT, DIGIT **13G10** and **10G9** were complexed with 5  $\mu$ g of mfluc in PBS 5.5 as described above. Aliquots containing the same dose of the DIGIT/mRNA were stored at –80 °C, and each week, an aliquot was tested via retro-orbital elivery to assess the integrity of the encapsulated mRNA by delivering retro-orbitally and measuring whole-body luminescence 6 h after injection.

### Hemolysis assay

Blood were isolated from balb/c mice in EDTA containing tubes and centrifuged at 4000 RPM for 10 min at 4 °C and washed twice with 1X PBS. Red blood cell pellets (30  $\mu$ l) were diluted with 1X PBS 1:10 and distributed into 1.5 mL Eppendorf tubes. The DIGIT or alcohol were added to the well and incubated at 37 °C for 20 min. The mixtures were centrifuged at 4000 RPM for 5 min and the absorbance of supernatant was measured on a transparent 96 well plate using a plate reader (Spectra i3x) at 540 nm.

### Statistical analysis

All statistical analysis was performed with Prism (GraphPad Software v9.2.0). All measurements were taken from distinct samples. For comparing two groups, *P*-values were determined using Student's *t*-tests (two-tailed). For comparing more than two groups, 2-way ANOVAs were applied. Differences between groups were considered significant for *P*-values < 0.05. No statistical methods were used to predetermine sample sizes. Mice were assigned to the various experimental groups randomly. Data collection and analysis were not blinded to the conditions of the experiments.

### Reporting summary

Further information on research design is available in the Nature Portfolio Reporting Summary linked to this article.

### Data availability

Source data are provided with this paper. Any remaining information can be obtained from the corresponding author upon reasonable request. Source data are provided with this paper.

### References

1. Sterner, E. Analyses of the 2023 Nobel Prize in Physiology or Medicine: Nucleoside Base Modifications and Effective mRNA Vaccines. *Sci. Technol. Libr.* **43**, 1–17 (2024).
2. Baden, L. R. et al. Efficacy and Safety of the mRNA-1273 SARS-CoV-2 Vaccine. *N. Engl. J. Med.* **384**, NEJMoa2035389 (2020).
3. Chaudhary, N., Weissman, D. & Whitehead, K. A. mRNA vaccines for infectious diseases: principles, delivery and clinical translation. *Nat. Rev. Drug Discov.* **20**, 817–838 (2021).
4. Sahin, U. et al. An RNA vaccine drives immunity in checkpoint-inhibitor-treated melanoma. *Nature* **585**, 107–112 (2020).
5. Moghimi, S. M. & Simberg, D. Pro-inflammatory concerns with lipid nanoparticles. *Mol. Ther.* **30**, 2109–2110 (2022).
6. Ju, Y. et al. Anti-PEG Antibodies Boosted in Humans by SARS-CoV-2 Lipid Nanoparticle mRNA Vaccine. *ACS Nano* **16**, acsnano.2c04543 (2022).
7. Ndeupen, S., Qin, Z., Jacobsen, S. & Igyarto, B. Z. The mRNA-LNP platform's lipid nanoparticle component used in preclinical vaccine studies is highly inflammatory. *J. Immunol.* **206**, 30.01–30.01 (2021).
8. Gillmore, J. D. et al. CRISPR-Cas9 in vivo gene editing for transthyretin amyloidosis. *N. Engl. J. Med.* **385**, 493–502 (2021).
9. Ramaswamy, S. et al. Systemic delivery of factor IX messenger RNA for protein replacement therapy. *Proc. Natl Acad. Sci.* **114**, E1941–E1950 (2017).
10. Xue, Y. et al. LNP-RNA-engineered adipose stem cells for accelerated diabetic wound healing. *Nat. Commun.* **15**, 739 (2024).
11. Wang, X. et al. Preparation of selective organ-targeting (SORT) lipid nanoparticles (LNPs) using multiple technical methods for tissue-specific mRNA delivery. *Nat. Protoc.* **18**, 265–291 (2023).
12. LoPresti, S. T., Arral, M. L., Chaudhary, N. & Whitehead, K. A. The replacement of helper lipids with charged alternatives in lipid nanoparticles facilitates targeted mRNA delivery to the spleen and lungs. *J. Control. Release* **345**, 819–831 (2022).
13. Riley, R. S. et al. Ionizable lipid nanoparticles for in utero mRNA delivery. *Sci. Adv.* **7**, eaba1028 (2021).

14. Melamed, J. R. et al. Ionizable lipid nanoparticles deliver mRNA to pancreatic  $\beta$  cells via macrophage-mediated gene transfer. *Sci. Adv.* **9**, eade1444 (2023).
15. Haabeth, O. A. W. et al. Local Delivery of Ox40L, Cd80, and Cd86 mRNA Kindles Global Anticancer Immunity. *Cancer Res* **79**, 1624–1634 (2019).
16. Zhang, X. et al. One-Component Cationic Lipids for Systemic mRNA Delivery to Splenic T Cells. *Angew. Chem.* **136**. <https://doi.org/10.1002/ange.202405444> (2024).
17. Zhang, D. et al. One-Component Multifunctional Sequence-Defined Ionizable Amphiphilic Janus Dendrimer Delivery Systems for mRNA. *J. Am. Chem. Soc.* **143**, 12315–12327 (2021).
18. McKinlay, C. J. et al. Charge-altering releasable transporters (CARTs) for the delivery and release of mRNA in living animals. *Proc. Natl Acad. Sci.* **114**, E448–E456 (2017).
19. Li, Z. et al. Charge-altering releasable transporters enhance mRNA delivery in vitro and exhibit in vivo tropism. *Nat. Commun.* **14**, 6983 (2023).
20. Blake, T. R. et al. Lysine-Derived Charge-Altering Releasable Transporters: Targeted Delivery of mRNA and siRNA to the Lungs. *Bioconjugate Chem.* **34**, 673–685 (2023).
21. Chen, R. et al. Engineering circular RNA for enhanced protein production. *Nat. Biotechnol.* **41**, 262–272 (2023).
22. Haabeth, O. A. W. et al. mRNA vaccination with charge-altering releasable transporters elicits human T cell responses and cures established tumors in mice. *Proc. Natl Acad. Sci.* **115**, E9153–E9161 (2018).
23. Amaya, L. et al. Circular RNA vaccine induces potent T cell responses. *Proc. Natl Acad. Sci.* **120**, e2302191120 (2023).
24. Li, Z. et al. Organ- and Cell-Selective Delivery of mRNA In Vivo Using Guanidylated Serinol Charge-Altering Releasable Transporters. *J. Am. Chem. Soc.* **146**, 14785–14798 (2024).
25. Omo-Lamai, S. et al. Physicochemical Targeting of Lipid Nanoparticles to the Lungs Induces Clotting: Mechanisms and Solutions. *Adv. Mater.* **36**, e2312026 (2024).
26. Brosnan, J. T. & Brosnan, M. E. Creatine metabolism and the urea cycle. *Mol. Genet. Metab.* **100**, S49–S52 (2010).
27. Gangopadhyay, D. et al. Raman spectroscopic approach to monitor the in vitro cyclization of creatine→creatinine. *Chem. Phys. Lett.* **618**, 225–230 (2015).
28. Stanzl, E. G., Trantow, B. M., Vargas, J. R. & Wender, P. A. Fifteen Years of Cell-Penetrating, Guanidinium-Rich Molecular Transporters: Basic Science, Research Tools, and Clinical Applications. *Acc. Chem. Res.* **46**, 2944–2954 (2013).
29. Geihe, E. I. et al. Designed guanidinium-rich amphipathic oligo-carbonate molecular transporters complex, deliver and release siRNA in cells. *Proc. Natl Acad. Sci.* **109**, 13171–13176 (2012).
30. Giese, M. W. & Lecher, C. S. Non-enzymatic cyclization of creatine ethyl ester to creatinine. *Biochem. Biophys. Res. Commun.* **388**, 252–255 (2009).
31. Hamada, Y. Novel prodrugs with a spontaneous cleavable guanidine moiety. *Bioorg. Med. Chem. Lett.* **26**, 1685–1689 (2016).
32. Lee, S. M. et al. A Systematic Study of Unsaturation in Lipid Nanoparticles Leads to Improved mRNA Transfection In Vivo. *Angew. Chem. Int. Ed.* **60**, 5848–5853 (2021).
33. Kim, H.-O., Mathew, F. & Ogbu, C. A Convenient Synthesis of Disubstituted Guanidines via the Mitsunobu Protocol. *Synlett* **1999**, 193–194 (1999).
34. Drake, B., Patek, M. & Lebl, M. A Convenient Preparation of Mono-substituted N,N'-di(Boc)-Protected Guanidines. *Synthesis* **1994**, 579–582 (1994).
35. Kenyon, C. L. & Rowley, G. L. Tautomeric Preferences among Glycocyamidines. *J. Am. Chem. Soc.* **93**, 5552–5560 (1971).
36. McKinlay, C. J., Benner, N. L., Haabeth, O. A., Waymouth, R. M. & Wender, P. A. Enhanced mRNA delivery into lymphocytes enabled by lipid-varied libraries of charge-altering releasable transporters. *Proc. Natl Acad. Sci.* **115**, E5859–E5866 (2018).
37. Lokugamage, M. P., Sago, C. D., Gan, Z., Krupczak, B. R. & Dahlman, J. E. Constrained Nanoparticles Deliver siRNA and sgRNA to T Cells In Vivo without Targeting Ligands. *Adv. Mater.* **31**, e1902251 (2019).
38. Schoenmaker, L. et al. mRNA-lipid nanoparticle COVID-19 vaccines: Structure and stability. *Int. J. Pharm.* **601**, 120586–120586 (2021).
39. Zhang, D. et al. The Unexpected Importance of the Primary Structure of the Hydrophobic Part of One-Component Ionizable Amphiphilic Janus Dendrimers in Targeted mRNA Delivery Activity. *J. Am. Chem. Soc.* **144**, 4746–4753 (2022).
40. Chen, J. et al. Combinatorial design of ionizable lipid nanoparticles for muscle-selective mRNA delivery with minimized off-target effects. *Proc. Natl Acad. Sci. U. S. A.* **120**, e2309472120 (2023).
41. Schober, G. B., Story, S. & Arya, D. P. A careful look at lipid nanoparticle characterization: analysis of benchmark formulations for encapsulation of RNA cargo size gradient. *Sci. Rep.* **14**, 2403 (2024).
42. Debbage, P. L. et al. Lectin Intravital Perfusion Studies in Tumor-bearing Mice: Micrometer-resolution, Wide-area Mapping of Microvascular Labeling, Distinguishing Efficiently and Inefficiently Perfused Microregions in the Tumor. *J. Histochem. Cytochem.* **46**, 627–639 (1997).
43. Zelepukin, I. V. et al. Fast processes of nanoparticle blood clearance: Comprehensive study. *J. Control. Release* **326**, 181–191 (2020).
44. Sabnis, S. et al. A novel amino lipid series for mRNA delivery: Improved endosomal escape and sustained pharmacology and safety in non-human primates. *Mol. Ther.* **26**, 1509–1519 (2018).
45. Li, Y.-X. et al. Targeting pulmonary vascular endothelial cells for the treatment of respiratory diseases. *Front. Pharmacol.* **13**, 983816 (2022).
46. Jiang, A. Y. et al. Combinatorial development of nebulized mRNA delivery formulations for the lungs. *Nat. Nanotechnol.* **19**, 364–375 (2024).
47. Cheng, M. H. Y. et al. Induction of Bleb Structures in Lipid Nanoparticle Formulations of mRNA Leads to Improved Transfection Potency. *Adv. Mater.* **35**, e2303370 (2023).
48. Kauffman, K. J. et al. Rapid, single-cell analysis and discovery of vectored mRNA transfection in vivo with a loxP-flanked tdTomato reporter mouse. *Mol. Ther. Nucleic Acids* **10**, 55–63 (2018).
49. O'Connell, K. E. et al. Practical murine hematopathology: a comparative review and implications for research. *Comp. Med.* **65**, 96–113 (2015).
50. Wender, P. A. et al. The design, synthesis, and evaluation of molecules that enable or enhance cellular uptake: Peptoid molecular transporters. *Proc. Natl Acad. Sci.* **97**, 13003–13008 (2000).
51. Siprashvili, Z. et al. Gene Transfer via Reversible Plasmid Condensation with Cysteine-Flanked, Internally Spaced Arginine-Rich Peptides. *Hum. gene Ther.* **14**, 1225–1233 (2003).

## Acknowledgements

This study was supported by NIH R01 AI161803 (P.A.W.), NIH R01CA245533 (P.A.W.), Stanford RNA Medicine Program (H.Y.C.), the Stanford Center for Molecular Analysis and Design (Z.L.), and Stanford Bio-X (L.A.), and the Stanford Office of the Vice Provost for Undergraduate Education (J.L.H.). H.Y.C. is an Investigator of the Howard Hughes Medical Institute. Technical support from the Veterinary Service Center (VSC) at Stanford Medicine and from Stanford SUMS for mass spectrometry analysis is gratefully acknowledged. We also thank Dr. Kerriann Casey and the Comparative Medicine team at the Veterinary Service Center, Stanford University, for providing the necropsy services for this study. We thank Stephen Lynch for help with NMR degradation studies and Harrison P. Rahn for providing hydrogenated isoprenoid lipids for DIGIT synthesis.

## Author contributions

Z.L. conceived the idea and designed the experiments with input from all co-authors. Z.L., A.E., and J.L.H. performed chemical synthesis and characterization. Z.L., L.A., S.K.W., and P.K.Y. performed animal studies. Z.L., L.A., A.E., H.Y.C. and P.A.W. wrote the manuscript with input from all co-authors.

## Competing interests

H.Y.C. is an employee and stockholder of Amgen as of Dec. 16, 2024. H.Y.C. is a co-founder of Accent Therapeutics, Boundless Bio, Cartography Biosciences, Orbital Therapeutics, and until Dec. 15, 2024, an advisor of Arsenal Biosciences, Chroma Medicine, Exai Bio, and Spring Science. P.A.W. is a co-founder of BryoLogyx and N1 Life and an advisor to Vaxanix, N1 Life, Synaptogenix, Cytokinetics, SuperTrans Medical, Ativo and Vault Pharma. The remaining authors declare no competing interests.

## Additional information

**Supplementary information** The online version contains supplementary material available at <https://doi.org/10.1038/s41467-025-62200-3>.

**Correspondence** and requests for materials should be addressed to Paul A. Wender.

**Peer review information** *Nature Communications* thanks Bowen Li and the other, anonymous, reviewer(s) for their contribution to the peer review of this work. A peer review file is available.

**Reprints and permissions information** is available at <http://www.nature.com/reprints>

**Publisher's note** Springer Nature remains neutral with regard to jurisdictional claims in published maps and institutional affiliations.

**Open Access** This article is licensed under a Creative Commons Attribution-NonCommercial-NoDerivatives 4.0 International License, which permits any non-commercial use, sharing, distribution and reproduction in any medium or format, as long as you give appropriate credit to the original author(s) and the source, provide a link to the Creative Commons licence, and indicate if you modified the licensed material. You do not have permission under this licence to share adapted material derived from this article or parts of it. The images or other third party material in this article are included in the article's Creative Commons licence, unless indicated otherwise in a credit line to the material. If material is not included in the article's Creative Commons licence and your intended use is not permitted by statutory regulation or exceeds the permitted use, you will need to obtain permission directly from the copyright holder. To view a copy of this licence, visit <http://creativecommons.org/licenses/by-nc-nd/4.0/>.

© The Author(s) 2025